1   **Inhibitors of VPS34 and lipid metabolism suppress SARS-CoV-2 replication**

2   Jesus A. Silvas, [1,3], Alexander S. Jureka[1,3], Anthony M. Nicolini[2], Stacie A. Chvatal[2], and

3   Christopher F. Basler[1*]

4   [1] Center for Microbial Pathogenesis, Institute for Biomedical Sciences, Georgia State University,

5   Atlanta, GA, 30303

6   [2] Axion BioSystems, Inc., Atlanta, GA 30309

7   [3] Equal contribution

8   *Corresponding Author
9   Christopher F. Basler PhD
10   Center for Microbial Pathogenesis
11   Institute for Biomedical Sciences
12   Georgia State University
13   Atlanta, GA 30307
14   (404) 413—3651
15   cbasler@gsu.edu
16

17

18

19

20

21

22

23

24

25   **ABSTRACT**

26   Therapeutics targeting replication of SARS coronavirus 2 (SARS-CoV-2) are urgently needed.

27   Coronaviruses rely on host membranes for entry, establishment of replication centers and egress.

28   Compounds targeting cellular membrane biology and lipid biosynthetic pathways have

29   previously shown promise as antivirals and are actively being pursued as treatments for other

30   conditions. Here, we tested small molecule inhibitors that target membrane dynamics or lipid

31   metabolism. Included were inhibitors of the PI3 kinase VPS34, which functions in autophagy,

32   endocytosis and other processes; Orlistat, an inhibitor of lipases and fatty acid synthetase, is

33   approved by the FDA as a treatment for obesity; and Triacsin C which inhibits long chain fatty

34   acyl-CoA synthetases. VPS34 inhibitors, Orlistat and Triacsin C inhibited virus growth in Vero

35   E6 cells and in the human airway epithelial cell line Calu-3, acting at a post-entry step in the

36   virus replication cycle. Of these the VPS34 inhibitors exhibit the most potent activity.

37

38

39

40

41

42

43

44

45

INTRODUCTION

SARS-CoV-2, a member of the *Betacoronavirus* genus, is an enveloped positive-sense, RNA virus responsible for a current pandemic[1]. Because of its profound impact on society and human health there is an urgent need to understand SARS-CoV-2 replication requirements and to identify therapeutic strategies[2]. Repurposing drugs developed for other purposes may provide a shortcut to therapeutic development[3-6]. The use of compounds known to target specific host factors may also elucidate key pathways needed for virus replication.

Coronavirus (CoV) replication involves multiple critical interactions with host cell membranes, including during viral entry and virus release[2, 7-9]. In addition, one of the most striking features of CoV infection is the establishment of replication organelles that consist of double membrane vesicles (DMV), double-membrane spherules (DMSs) and convoluted membranes (CM) with DMVs serving as the main site of viral RNA synthesis[10]. The origin of these membrane organelles in beta-coronavirus infection remains incompletely understood. The membrane structures colocalize with LC3, a protein with well-known functions in autophagy[7, 11]. In murine embryonic stem cell lines, autophagy was found to be critical for DMV formation and replication of the beta-coronavirus mouse hepatitis virus[7]. However, studies in bone marrow derived macrophages or primary mouse embryonic fibroblasts lacking ATG5 indicated that autophagy is not essential for DMV formation or MHV replication[11]. An alternate model indicates that beta coronaviruses usurp vesicles known as EDEMosomes, which associate with non-lipidated LC3 and normally function to regulate ER-associated degradation (ERAD), to provide membranes for replication[8].

Many enveloped, positive-sense RNA viruses that replicate in double membrane compartments have been demonstrated to be sensitive to inhibitors of various aspects of

69   membrane metabolism/biology. For example, VPS34 a class III phosphoinositol-3 kinase (PI3K)

70   that plays roles in autophagy, endosomal trafficking, and other aspects of membrane biology has

71   been implicated in the replication of hepatitis C virus (HCV) and tombusvirus (TBSV)[12, 13]. The

72   compound Triacsin C, which inhibits an enzyme upstream of triglyceride synthesis, long chain

73   fatty acyl CoA, impairs the growth of several viruses that require for replication lipid droplets,

74   organelles that serve as storage sites for neutral lipids such as triacylglycerol[14-16]. Downstream of

75   long chain fatty acyl CoA in the synthesis of triglycerides are diacylglycerol acyltransferases 1

76   and 2 (DGAT1 and DGAT2). Inhibition of these enzymes inhibits HCV and rotavirus

77   replication. More general inhibitors of fatty acid synthetase such as Orlistat, also decrease

78   replication of several different viruses[17-20].

79   Here we asked whether SARS-CoV-2 is susceptible to modulators of lipid metabolism by

80   assessing the sensitivity of the virus in Vero E6 and Calu-3 cells to VPS34 inhibitors, Triacsin C,

81   inhibitors of DGATs and Orlistat, an inhibitor of FASN[21]. We find that two inhibitors of VPS34

82   potently inhibited SARS-CoV-2 replication, whereas an FDA-approved inhibitor of a different

83   class of PI3K had minimal effect on replication. Targeting FASN and *de novo* synthesis of

84   triacylglycerol, diacylglycerol and cholesterol esters each impairs SARS-CoV-2 replication

85   whereas inhibition of DGATs was not effective. We also identified that each inhibitor exhibits

86   antiviral effects post-entry and that they perturb the structure of viral replication centers. Taken

87   together, the data presented here implicates specific lipid metabolism pathways in SARS-CoV-2

88   replication and suggests that these pathways are promising therapeutic targets.

89

90   **MATERIALS AND METHODS**

Virus and cell lines

Vero E6 (ATCC# CRL-1586), Calu-3 (ATCC# HTB-55), and Caco-2 (ATCC# HTB-37) were maintained in DMEM (Corning) supplemented with 10% heat inactivated fetal bovine serum (FBS; GIBCO). Cells were kept in a 37°C, 5% CO_2 incubator without antibiotics or antimycotics. SARS-CoV-2, strain USA_WA1/2020, was obtained from the World Reference Collection for Emerging Viruses and Arboviruses at the University of Texas Medical Branch-Galveston.

Virus Propagation and Plaque Assays

A lyophilized ampule of SARS-CoV-2 was initially resuspended in DMEM supplemented with 2% FBS. VeroE6 cells were inoculated in duplicate with a dilution of 1:100 with an adsorption period of 1 hour at 37C and shaking every 15 minutes. Cells were observed for cytopathic effect (CPE) every 24 hours. Stock SARS-CoV-2 virus was harvested at 72 hours post infection (h.p.i) and supernatants were collected, clarified, aliquoted, and stored at -80°C.

For plaque assays, Vero E6 cells were seeded onto a 24-well plate 24 hours before infection. 100ul of SARS-CoV-2 serial dilutions were added, adsorbed for 1 hour at 37C with shaking at 15-minute intervals. After the absorption period, 1 mL of 0.6% microcrystalline cellulose (MCC; Sigma 435244) in serum-free DMEM was added. To stain plaque assays MCC was removed by aspiration, and 10% neutral buffered formalin (NBF) added for one hour at room temp and then removed. Monolayers were then washed with water and stained with 0.4% crystal violet. Plaques were quantified and recorded as plaque forming units (PFU)/mL.

Confocal microscopy

112   For confocal microscopy analysis, all cell lines were pre-seeded 24 hours before infection

113   onto glass coverslips and infected with SARS-CoV-2 at a multiplicity of infection (MOI) of 1. At

114   24 hours post-infection (h.p.i.) supernatant was removed, and samples fixed with 10% NBF for 1

115   hour at room temperature followed by PBS wash and permeabilized with sterile filtered 0.1%

116   Saponin in PBS. Cells were blocked with 0.1% Saponin in Fluorescent Blocker (ThermoFisher)

117   for 1 hour at RT. Primary antibodies were added and incubated overnight at 4C. AlexaFluor488,

118   594, and 647 conjugated secondary antibodies were used and nuclei stained with DAPI. Samples

119   were imaged on Zeiss LSM800 Confocal with Super Resolution AiryScan. Images were

120   rendered in ZenBlue or Imaris Viewer 9.0.

121   **Maestro Z Impedance Experiments**

122   Prior to cell plating, CytoView-Z 96-well electrode plates (Axion BioSystems, Atlanta,

123   GA) were coated with 5 µg/mL human fibronectin (Corning) for 1 hr at 37C. After coating,

124   fibronectin was removed and 100 µL of DMEM/10% FBS was added to each well. The plate was

125   then docked into the Maestro Z instrument to measure impedance electrode baseline. Vero E6

126   cells were then plated to confluency (~75,000 cells/well) in the coated CytoView-Z plates and

127   left at room temperature for 1 hour to ensure even coverage of the well. Plates containing Vero

128   E6 cells were then docked into the Maestro Z for 24 hours at 37°C/5% CO_2 to allow the cells to

129   attach and the monolayer to stabilize, as measured by resistance, a component of impedance. The

130   Maestro Z was used to monitor the resistance of the monolayer as it formed, very similar to

131   transepithelial electrical resistance (TEER)[22]. In this study, resistance was measured at 10 kHz,

132   which reflects both cell coverage over the electrode and strength of the barrier formed by the cell

133   monolayer. For compound treatments, media was removed from wells of the CytoView-Z plates

134   and 195 µL of pre-warmed DMEM/2% FBS was added with the indicated concentration of

135   compound. Infections with SARS-CoV-2 at an MOI of 0.01 were carried out by directly adding

136   5 μL of virus to each well. Plates were then docked within the Maestro Z and resistance

137   measurements were continuously recorded for 48-72 hours post-infection. All plates contained

138   media only, full lysis, uninfected, and SARS-CoV-2 infected controls. For calculation of percent

139   inhibition, raw resistance values for each well were normalized to the value at 1 hour post-

140   infection within the Axis Z software, and percent inhibition was calculated with the following

141   formula: Percent Inhibition = 100*(1-(1- average of treated cells)/(1-average of infected

142   control)). Median time to death calculations were performed by fitting the Boltzmann sigmoid

143   equation to raw kinetic resistance data in Graphpad Prism. Fifty percent maximum velocity

144   (V50) values obtained from the Boltzmann sigmoid fits were used to determine median time to

145   death for each MOI.

146   **Cell viability assay**

147   VeroE6 or Calu-3 cells were seeded in 96-well black walled microplates and incubated

148   overnight. Cells were then treated with compounds and CellTox Green Dye (Promega) to

149   monitor compound cytotoxicity. Fluorescence (Excitation: 485nm, Emission: 520nm) was

150   measured every 24 hours post treatment for 3 days. Percent viability was determined using the

151   minimum fluorescence obtained from media only cells and the maximum value obtained by cells

152   lysed with 1% Triton-X.

153   **Labeling of nascent viral RNA**

154   VeroE6 cells were seeded onto glass coverslips and incubated overnight at 37C. Cells

155   were then infected with SARS-CoV-2 at an MOI of 3. At 24 h.p.i. cells were treated with 1μM

156   of Actinomycin D (Sigma) for 1 hour. Nascent RNA was labeled using Click-iT™ RNA

157 Alexa Fluor™ 594 Imaging Kit (ThermoFisher). Cells were then processed for confocal

158 analysis.

159 **Compounds**

160 VPS34 IN-1 (#17392), PIK-III (#17002), Triacsin C (#10007448), and

161 Orlistat (#10005426) were purchased from Cayman Chemical (Ann Arbor,

162 Michigan). Remdesivir was purchased from Target Molecule Corp. (T7766, Boston,

163 Massachusetts). T863 (#SML0539) and PF06424439 (#PZ0233) were purchased from Sigma-

164 Aldrich (St. Louis, Missouri). All chemicals were resuspended in dimethylsulfoxide

165 (DMSO). [23]

166 **RESULTS**

167 **Development of 96-well format assay to measure SARS-CoV-2 cytopathic effects**

168 SARS-CoV-2 induces significant cytopathic effects in infected Vero E6 cells. Based on

169 this property, we standardized a 96-well format assay that provides continuous real-time, label-

170 free monitoring of the integrity of cell monolayers, thereby providing assessment of virus growth

171 through decreased cell viability. This assay was standardized using the Maestro Z platform

172 (Axion BioSystems, Atlanta, GA), an instrument that uses 96-well plates containing electrodes in

173 each well (CytoView-Z plates). The electrodes measure electrical impedance across the cell

174 monolayer every minute throughout the course of the experiment. As SARS-CoV-2 replication

175 damages the cell monolayer, impedance measurements decrease over time, providing a detailed

176 assessment of infection kinetics.

177 The capacity of the system to differentiate different levels of virus replication was first

178 assessed. Confluent Vero E6 monolayers in CytoView-Z plates were infected with SARS-CoV-2

179   at multiple MOIs (10 to 0.0001) and resistance measurements were acquired for 72 hours post-

180   infection. As shown in **Figure 1A,** the progression of infection at each MOI was clearly distinct.

181   A decrease in resistance could be observed as early as 18-20 h.p.i. at an MOI of 10 and 1, and as

182   late as 56 h.p.i. at an MOI of 0.0001. Depending on MOI, signals reached their nadirs between

183   32 to 72 h.p.i. To correlate with a decrease in resistance, the raw kinetic data was used to

184   determine the median time to cell death for each MOI **(Figure 1B)**. Based on its desirable

185   kinetics, the MOI of 0.01 was chosen for the screening of compounds for antiviral activities.

186   To establish the Maestro Z as a potential instrument for screening of anti-SARS-CoV-2

187   therapeutics, we first tested Remdesivir, a well-described inhibitor of SARS-CoV-2 that has been

188   granted emergency use authorization (EUA) for the treatment of COVID-19[24, 25]. Vero E6 cells

189   were seeded on a CytoView-Z plate, incubated overnight to allow cells to stabilize, pretreated

190   with 6-fold dilutions of Remdesivir for 1 hour and infected with SARS-CoV-2. Resistance

191   measurements were recorded for 48 h.p.i. **(Figure 1C)**. In agreement with previous studies, we

192   determined an 50% inhibitory concentration (IC50) for Remdesivir of 1.54 μM **(Figure 1D)**[24].

193   Taken together, these data validate the impedance-based assay described as a tool for screening

194   of potential SARS-CoV-2 therapeutics.

195   **Inhibitors of VPS34 activity impair SARS-CoV-2 growth**

196   VPS34 is a multifunctional protein involved in autophagy and membrane trafficking.

197   Since coronaviruses induce formation of double membrane vesicles for replication, we wanted to

198   determine if VPS34 activity was essential for SARS-CoV-2 replication. Therefore, we tested two

199   well characterized VPS34 inhibitors IN-1 (referred as VPS34-IN1 below) and PIK-III over a 10-

200   point dose response in the resistance assay[26]. The compounds were added to pre-plated Vero E6

201   cells 1 hour prior to infection with SARS-CoV-2 at a MOI of 0.01. Both VPS34-IN1 and PIK-III

202   induced rapid cytotoxicity at 50 µM and 16.67 µM as indicated by a rapid decrease in resistance

203   measurements between 1 and 20 h.p.i. **(Figure 2A and 2C)**. However, at concentrations of 5.56

204   µM and below, the integrity of the monolayer was preserved relative to the mock-treated control

205   indicating an antiviral effect and an absence of cytotoxicity. Calculations based on normalized

206   resistance measurements at 48 h.p.i for non-toxic doses yielded IC50s of 0.29uM for VPS34-IN1

207   and 0.202uM for PIK-III **(Figure 2B and 2D, respectively)**. Additionally, IC90s of 2.52 µM

208   (VPS34-IN1) and 1.81 µM (PIK-III) were also calculated. These data suggest that the VPS34

209   kinase plays a significant role in SARS-CoV-2 replication and is a potential target for therapeutic

210   intervention.

211   **Inhibition of fatty acid metabolism inhibits SARS-CoV-2 replication**

212   Fatty acid metabolism leads to production of triglycerides, phospholipids and other

213   molecules[27]. Elongation of the phospholipid membranes can be aided by channeling fatty acid

214   into phospholipid synthesis[28]. Modulation of fatty acid metabolism has been shown to impact

215   several viruses such as dengue virus, hepatitis C virus, and Old World alphaviruses[18, 29, 30]. Two

216   well-described compounds that inhibit fatty acid metabolism are Orlistat and Triacsin C, both of

217   which have been shown to have antiviral activity[19, 30]. Orlistat is an FDA-approved drug that

218   inhibits lipases and also fatty acid synthase (FASN), and Triacsin C inhibits long chain Acyl-

219   CoA synthetases. To test these against SARS-CoV-2, VeroE6 cells were pre-seeded onto a

220   CytoView-Z plate, allowed to stabilize and then pre-treated with Triacsin C or Orlistat for 1 hour

221   before infection with SARS-CoV-2 at an MOI of 0.01. Based on the toxicity window of 1-20

222   h.p.t. determined with the VPS34 inhibitors, neither Triacsin C nor Orlistat induced early

223   cytotoxic effects, even at the highest concentrations of 50uM and 500uM, respectively **(Figure**

224   **3A and 3C)**. Both compounds exhibited inhibition at the higher concentrations tested, although

225 complete inhibition was not achieved even with 500 µM of Orlistat. Based on the data we

226 extrapolated an IC50 of 422.3uM for Orlistat and calculated an IC50 of 19.5uM for Triacsin C

227 **(Figure 3B and 3D)**. Viruses such as HCV and rotavirus that are sensitive to inhibition by

228 Triacsin C are also impaired by inhibitors of DGATs[14, 31]. Therefore, we tested the effects of

229 DGAT1 and DGAT2 inhibitors T863 and PF06424439[32, 33]. Neither compound displayed any

230 inhibitory activity (**Supplemental Figure 1**). This data suggests that metabolism of fatty acids

231 plays an important role in SARS-CoV-2 infection.

232 **VPS34 inhibitors exhibit potent attenuation of SARS-CoV-2 early and late in its replication**

233 **cycle**

234 Next, time-of-addition studies were performed. We sought to determine how long the

235 addition of VPS34-IN1, PIK-III, Orlistat, or Triacsin C could be postponed before activity was

236 lost. Additionally, this would identify if the anti-viral activity of each compound impacted a pre-

237 or post- viral entry step. As indicated in **Figure 4A**, 4 conditions were tested 1) single treatment

238 1 hour prior to viral infection, with compound removed just prior to infection; 2) 1 hour pre-

239 treatment with continuous dosing; 3) dosing at 2 h.p.i.; and 4) dosing at 4 h.p.i.. VeroE6 cells

240 were pre-seeded onto a CytoView-Z plate and allowed to stabilize, compounds were added, and

241 resistance was monitored for 48 hours after infection. Percent inhibition was calculated based on

242 resistance values at 48 h.p.i. We observed that a single 5 µM treatment of VPS34-IN1 or PIK-III

243 inhibited SARS-CoV-2 replication **(Figure 4B)**. Additionally, inhibition was observed even

244 when added after 4 h.p.i. In contrast, removal of Orlistat or Triacsin C before infection,

245 eliminated their efficacy. Maintenance throughout the experiment was inhibitory, as was addition

246 at 2 or 4 hours post infection. Interestingly, delayed treatment with Triacsin C at 50µM exhibited

247 greater anti-viral activity that initiating the treatment one hour prior to infection. Altogether,

248   these data demonstrate activity of the VPS34 inhibitors at both early and late, post-entry time

249   points and indicate that the effects of Orlistat and Triacsin C are likely post-entry.

250   **Attenuation of VPS34 kinase activity and fatty acid metabolism inhibit SARS-CoV-2**

251   **in a human airway epithelial cell line**

252   We proceeded to investigate if the inhibitors were effective in the human lung carcinoma

253   cell line, Calu-3, by directly measuring production of infectious virus and cytotoxicity. That this

254   cell line is derived from the human airway and is highly susceptible to infection has established it

255   as a standard for infection studies with SARS-CoV-1, MERS-CoV and SARS-CoV-2[34, 35]. Calu-

256   3 cells were plated onto 96-well plates and allowed to reach 95% confluency. Cells were then

257   pre-treated with a range of concentrations of VPS34-IN1, PIK-III, Triacsin C, Orlistat, DMSO,

258   or mock treated with media alone for 1 hour then infected with SARS-CoV-2 at an MOI of 0.01.

259   Supernatants were collected at 48 h.p.i. and titered on VeroE6 cells by plaque assay. In parallel,

260   to determine cytotoxicity of these compounds, Calu-3 cells were seeded onto 96-well black

261   walled 96-well plates, allowed to reach 95% confluency and treated with VPS34-IN1, PIK-III,

262   Triacsin C, Orlistat, DMSO, or mock treated with media alone. CellTox Green was added at the

263   time of dosing and fluorescence measured at 48 h.p.i. in order to assess cytotoxicity. Each of the

264   compounds inhibited production of infectious virus, as measured by plaque assay on Vero E6

265   cells **Figure 5A, C, E, and G)**. In contrast to VeroE6 cells, no cytotoxicity was observed even at

266   the highest dose for each compound in Calu-3 cells. We observed IC50s of 0.55μM (VPS34-

267   IN1), 0.12μM (PIK-III), 21.25μM (Orlistat), and 0.04μM (Triacsin C), as shown in **Figure 5B,**

268   **D, F, and H**, respectively. Importantly, the IC50s calculated for VPS34-IN1 and PIK-III by

269   measuring infectious virus are in close agreement with IC50s calculated in Vero E6 cells using

270   the resistance-based assay. The IC50s for Triacsin C and Orlistat were substantially lower than in

271   the Vero cells. These data suggest that attenuation of the kinase activity of VPS34, synthesis of

272   fatty acids or production of long chain fatty acyl-CoA in human bronchial epithelial cells inhibits

273   replication of SARS-CoV-2.

274   VPS34 is a class III PI3 kinase. We therefore extended our study to determine if

275   BYL719, an FDA approved inhibitor of class I PI3 kinase used to treat breast cancer, would also

276   inhibit SARS-CoV-2 replication in Calu-3 cells. Unlike the VPS34-specific inhibitors, little

277   inhibition was detected up to 16.6 µM, at which we observed a 1-log decrease in viral titers

278   **(Supplemental Figure 2)**. This data suggests that not all PI3K classes play a significant role

279   during SARS-CoV-2 replication.

280   **Inhibition of VPS34 kinase activity and fatty acid metabolism disperse SARS-CoV-2**

281   **replication centers**

282   SARS-CoV-1 and MERS-CoV replicate in double membrane compartments to which the

283   autophagy membrane marker LC3 localizes[8, 9, 23]. We investigated if, similar to SARS-CoV-1

284   and MERS, SARS-CoV-2 nascent viral RNA and N co-localized with LC3. VeroE6 cells were

285   infected with SARS-CoV-2 at a MOI of 3 and at 24 h.p.i., were treated with 1µM of actinomycin

286   D to arrest host-cell transcription. Cells where then chased for 4 hours with 5-ethynyl uridine

287   (EU). Viral nascent RNA labeled during the EU chase was then detected with click chemistry,

288   indirect immunofluorescence performed using primary antibodies against N and LC3, and the

289   endoplasmic reticulum (ER) was detected with DPX BlueWhite ER stain. We observed distinct

290   formation of ring-like structures positive for ER, N, LC3, and nascent viral RNA **(Supplemental**

291   **Figure 3A)**. Co-localization analysis demonstrated that nascent viral RNA co-localized with N

292   or LC3 **(Supplemental Figure 3B).** This data demonstrates the presence of SARS-CoV-2

293   replication centers that form in association with LC3.

294 Because each compound exhibited inhibitory effects when added after viral entry, we

295 next asked whether the compounds altered the establishment of viral replication centers. Calu-3

296 cells were seeded onto fibronectin coated glass cover slips and allowed to reach 95% confluency.

297 Cells were pre-treated with approximately the IC90 of VPS34-IN1 (5 µM), PIK-III (5 µM),

298 Orlistat (500 µM), or Triacsin C (50 µM) and infected with SARS-CoV-2 at a MOI of 3. At 24

299 h.p.i. cells were fixed, permeabilized, and indirect immunofluorescence performed using primary

300 antibodies against SARS-CoV-2 nucleoprotein (N) and dsRNA. We observed that when

301 compared to the media only or DMSO controls, N became completely cytoplasmic and did not

302 form any large inclusion like formations in the presence of the compounds **(Figure 6)**.

303 Additionally, even though dsRNA could be detected both distributed throughout the cytoplasm

304 and associated with N in large inclusion like formations in the media only and DMSO controls,

305 in the cells treated with inhibitors, dsRNA was only found distributed throughout the cytoplasm.

306 This data suggests that the compound disrupt replication center formation.

307 **DISCUSSION**

308 Here, we demonstrate that two VPS34 inhibitors, Orlistat, and Triacsin C each have clear effects

309 on SARS-CoV-2 replication and the morphology of viral replication centers. Generation of

310 replication centers is a key feature of the replication of many viruses[36-38]. These can serve as sites

311 where required components concentrate within a relatively closed environment and hide viral

312 replication products from the host innate immune response[39]. In order to generate these centers,

313 many viruses usurp host cellular pathways that are used to generate membranes or organelles[38].

314 *Betacoronaviruses* have been shown to target the ERAD-EDEMosome-ER pathways to generate

315 double-membrane vesicles required for their replication[8]. The data presented here suggests roles

316 for VPS34, FASN, and long chain fatty acyl CoA in replication center formation and stability

317   suggesting a role for these host factors in providing the membranes needed for SARS-CoV-2

318   replication organelles.

319   VPS34 is of interest as a therapeutic target for a variety of conditions, including aging,

320   neurodegeneration and cancer[40, 41]. The two VPS34 inhibitors tested were VPS34-IN1 and PIK-

321   III which have *in vitro* IC50s for VPS34 of 25 nM and 18 nM, respectively[26, 42]. These were the

322   most potent compounds versus SARS-CoV-2 tested in this study. Each displayed an IC50 of less

323   than 1µM in either Vero E6 cells or Calu-3 cells. Activity in the Vero E6 cells was measured

324   based on the capacity of the compounds to prevent viral cytopathic effects as measured by

325   resistance across the cell monolayer, whereas the Calu-3 cell assay measured inhibition of

326   production of infectious virus particles. The resistance-based assay provided a built-in measure

327   of cell viability and integrity of the cell monolayer, providing assurance that decreases in

328   resistance measurements initially post-infection were not reflective of cytopathic effects. We also

329   independently determined that the compounds tested were non-toxic in Calu3 cells, likewise

330   demonstrating that decreases in viral titer were not due to compound toxicity. Based on the Calu-

331   3 data, the selectivity indices (SI) (CC50/IC50) for the compounds are >90 and >416 for VPS34-

332   IN1 and PIK-III, respectively.

333   VPS34 is a phosphoinositide kinase that functions in autophagy, endosomal trafficking

334   and other cellular functions[43]. VPS34 associates with VPS15 as well as with other proteins to

335   carry out its activities. One VPS34-containing complex, Complex I, includes VPS34, VPS15,

336   Beclin 1 and ATG14 and is critical for autophagosome formation. Complex II includes VPS34,

337   VPS15, Beclin 1 and UVRAG and functions in autophagosome-lysosome fusion and in

338   regulation of endosomes and multivesicular bodies[43]. While our inhibitor studies do not

339   differentiate between the various functions of VPS34 that might be involved in SARS-CoV-2

340 replication,. Autophagy has been implicated as necessary for MHV replication, however,

341 subsequent studies in different cell types suggest autophagy is not essential for MHV growth[7, 11].

342 Further, recent studies suggest that coronaviruses interfere with autophagy and that activation of

343 autophagy can inhibit replication of SARS-CoV, MERS CoV, and SARS-CoV-2[44, 45]. Given that

344 inhibition of VPS34 results in the inhibition of autophagy[26, 42], it would be expected that

345 inhibition of VPS34 would eliminate these anti-CoV effects of autophagy and promote SARS-

346 CoV-2 replication. Therefore, the disruptions in SARS-CoV-2 replication due to VPS34

347 inhibition described here may, instead, reflect inhibition of non-autophagy related functions of

348 VPS34.

349 Separate from autophagy, VPS34 has several other roles including in endosomal trafficking

350 and retrograde endosome-to-Golgi transport[43]. For the positive-sense RNA virus TBSV, VPS34

351 was implicated in providing phosphatidylethanolamine-enriched membranes for formation of

352 TBSV replication centers[13]. Based on our observation that VPS34 inhibitors disrupt the structure

353 of SARS-CoV-2 replication centers, it is possible that VPS34 functions to facilitate membrane

354 availability for SARS-CoV-2 replication organelle formation. Disruption of endocytic trafficking

355 might also explain our observation that pre-treatment with VPS34 inhibitors alone had

356 significant effects on SARS-CoV-2 replication.

357 Orlistat (tetrahydrolipstatin) is an FDA-approved weight loss drug that is taken orally and

358 inhibits gastric and pancreatic lipases in the digestive tract, reducing uptake of lipids[21]. Orlistat

359 also inhibits fatty acid synthase (FASN)[46]. Orlistat and other FASN inhibitors have previously

360 been examined for their anti-cancer and antiviral activities. Although the clinically approved oral

361 administration of Orlistat does not result in its significant systemic distribution, pre-clinical

362 studies in mice have demonstrated that systemic administration of Orlistat is well tolerated[47].

363   Orlistat has been demonstrated to have activity against several viruses, including varicella-zoster

364   virus (VZV), coxsackievirus B3 virus (CVB3), dengue virus (DENV), and other flaviviruses.

365   DENV uses it nonstructural protein 3 to recruit FASN to viral replication sites and enhances

366   synthesis of fatty acids[48]. As in our study, flaviviruses were sensitive to relatively high

367   concentrations of Orlistat and antiviral effects could be demonstrated when Orlistat was added to

368   cells post-infection[17]. Virus inhibition has typically been demonstrated at relatively high

369   concentrations of Orlistat, such as 100μM or higher for CVB3, and between 10μM and 84μM for

370   DENV3, depending on the timepoint post-infection DENV3 replication was measured[17, 19, 49].

371   For DENV3, the effect of Orlistat appeared to be after the early stages of infection[18]. This may

372   reflect the need for DENV to recruit FASN to sites of virus replication and to upregulate fatty

373   acid synthesis[48, 50]. It will be of interest to determine whether SARS-CoV-2 similarly depends on

374   an upregulation of fatty acid synthesis.

375   Triacsin C inhibits long chain fatty acid acyl-CoA synthetase. Interestingly, the long chain

376   fatty acid acyl-CoA synthetase ACSL3 was identified as an interactor of SARS-CoV-2 non-

377   structural protein 7, suggesting a role for this enzyme in virus replication[51]. Triacsin C also has

378   demonstrated antiviral activity for HCV and rotavirus[14-16]. For both HCV and rotavirus, the

379   antiviral effects of Triacsin C have been linked to reliance of these viruses on lipid droplets for

380   their replication[14-16]. Lipid droplets are organelles that store neutral lipids of which triglycerides

381   are a major component[52]. By inhibiting long chain fatty acyl CoA, Triacsin C blocks lipid droplet

382   formation. That antiviral activity against HCV and rotavirus is connected to lipid droplet

383   formation is supported by the fact that these viruses are sensitive to inhibition by the DGAT

384   inhibitors, T863 and PF06424439. In contrast, the compounds did not exhibit any activity against

385   SARS-CoV-2 in Vero E6 cells whereas Triacsin C did. This suggests an alternate role for long

386   chain fatty acyl CoA or its downstream metabolites other than triacylglycerol and lipid droplets.

387   It is notable that the IC50 for Triacsin C was substantially lower in the Calu-3 cell assay as

388   compared to the Vero cell assay. A lesser decrease in IC50 was also noted for Orlistat in the

389   Calu-3 cells versus the Vero E6 cells. These observations may reflect different degrees of

390   dependence of the virus on fatty acid metabolism in different cell types. From the perspective of

391   antiviral development, it is encouraging that the human airway-derived cells are the more

392   sensitive system given that SARS-CoV-2 targets the respiratory tract. Triacsin C has been

393   administered to mice daily for up to two months without overt signs of significant toxicity and

394   resulted in a decrease in atherosclerosis[53]. However, the pharmacokinetics and cell penetrance of

395   Triacsin C are viewed as significant impediments to its clinical use[54]. Despite this, Triacsin C

396   analogs have been developed[15], and long chain fatty acyl CoA synthetases are of interest as

397   potential therapeutics for cancer as well as for viruses[54].

398   Cumulatively, these data support lipid metabolism as a potential therapeutic target for SARS-

399   CoV-2 infection. The specific mechanisms by which VPS34 promotes SARS-CoV-2 replication

400   and the precise manner in which the VSP34 inhibitors impair replication warrant further

401   investigation. Additionally, the specific enzymes and products of fatty acid metabolism

402   necessary for efficient SARS-CoV-2 growth in human airway epithelial cells should be further

403   explored to more precisely identify relevant targets for therapeutic targeting. Further, it will be of

404   interest to understand the relative efficacies of inhibitors of fatty acid metabolism in different cell

405   types.

406

411   **Competing Interests.** Authors A.M.N. and S.A.C. are employees of Axion BioSystems who

412   provided the Axion Maestro Z instrument used in these studies.

413

References

1. Lundstrom, K. Coronavirus Pandemic-Therapy and Vaccines. *Biomedicines* **8** (2020).

2. Wang, L., Wang, Y., Ye, D. & Liu, Q. Review of the 2019 novel coronavirus (SARS-CoV-2) based on current evidence. *Int J Antimicrob Agents* **55**, 105948 (2020).

3. García-Serradilla, M., Risco, C. & Pacheco, B. Drug repurposing for new, efficient, broad spectrum antivirals. *Virus Res* **264**, 22-31 (2019).

4. Pizzorno, A., Padey, B., Terrier, O. & Rosa-Calatrava, M. Drug Repurposing Approaches for the Treatment of Influenza Viral Infection: Reviving Old Drugs to Fight Against a Long-Lived Enemy. *Front Immunol* **10**, 531 (2019).

5. Saini, K.S. *et al.* Repurposing anticancer drugs for COVID-19-induced inflammation, immune dysfunction, and coagulopathy. *Br J Cancer* (2020).

6. Li, G. & De Clercq, E. Therapeutic options for the 2019 novel coronavirus (2019-nCoV). *Nat Rev Drug Discov* **19**, 149-150 (2020).

7. Prentice, E., Jerome, W.G., Yoshimori, T., Mizushima, N. & Denison, M.R. Coronavirus replication complex formation utilizes components of cellular autophagy. *J Biol Chem* **279**, 10136-10141 (2004).

8. Reggiori, F. *et al.* Coronaviruses Hijack the LC3-I-positive EDEMosomes, ER-derived vesicles exporting short-lived ERAD regulators, for replication. *Cell Host Microbe* **7**, 500-508 (2010).

9. Reggiori, F., de Haan, C.A. & Molinari, M. Unconventional use of LC3 by coronaviruses through the alleged subversion of the ERAD tuning pathway. *Viruses* **3**, 1610-1623 (2011).

10. Snijder, E.J. *et al.* A unifying structural and functional model of the coronavirus replication organelle: Tracking down RNA synthesis. *PLoS Biol* **18**, e3000715 (2020).

11. Zhao, Z. *et al.* Coronavirus replication does not require the autophagy gene ATG5. *Autophagy* **3**, 581-585 (2007).

12. Su, W.C. *et al.* Rab5 and class III phosphoinositide 3-kinase Vps34 are involved in hepatitis C virus NS4B-induced autophagy. *J Virol* **85**, 10561-10571 (2011).

13. Feng, Z., Xu, K., Kovalev, N. & Nagy, P.D. Recruitment of Vps34 PI3K and enrichment of PI3P phosphoinositide in the viral replication compartment is crucial for replication of a positive-strand RNA virus. *PLoS Pathog* **15**, e1007530 (2019).

14. Liefhebber, J.M., Hague, C.V., Zhang, Q., Wakelam, M.J. & McLauchlan, J. Modulation of triglyceride and cholesterol ester synthesis impairs assembly of infectious hepatitis C virus. *J Biol Chem* **289**, 21276-21288 (2014).

15. Kim, Y. *et al.* Novel triacsin C analogs as potential antivirals against rotavirus infections. *Eur J Med Chem* **50**, 311-318 (2012).

16. Cheung, W. *et al.* Rotaviruses associate with cellular lipid droplet components to replicate in viroplasms, and compounds disrupting or blocking lipid droplets inhibit viroplasm formation and viral replication. *J Virol* **84**, 6782-6798 (2010).

17. Hitakarun, A. *et al.* Evaluation of the antiviral activity of orlistat (tetrahydrolipstatin) against dengue virus, Japanese encephalitis virus, Zika virus and chikungunya virus. *Sci Rep* **10**, 1499 (2020).

18. Tongluan, N. *et al.* Involvement of fatty acid synthase in dengue virus infection. *Virol J* **14**, 28 (2017).

19. Ammer, E. *et al.* The anti-obesity drug orlistat reveals anti-viral activity. *Med Microbiol Immunol* **204**, 635-645 (2015).

20. Esser, K. *et al.* Lipase inhibitor orlistat prevents hepatitis B virus infection by targeting an early step in the virus life cycle. *Antiviral Res* **151**, 4-7 (2018).

21. Heck, A.M., Yanovski, J.A. & Calis, K.A. Orlistat, a new lipase inhibitor for the management of obesity. *Pharmacotherapy* **20**, 270-279 (2000).

22. Benson, K., Cramer, S. & Galla, H.J. Impedance-based cell monitoring: barrier properties and beyond. *Fluids Barriers CNS* **10**, 5 (2013).

23. Prentice, E., McAuliffe, J., Lu, X., Subbarao, K. & Denison, M.R. Identification and characterization of severe acute respiratory syndrome coronavirus replicase proteins. *J Virol* **78**, 9977-9986 (2004).

24. Gordon, C.J. *et al.* Remdesivir is a direct-acting antiviral that inhibits RNA-dependent RNA polymerase from severe acute respiratory syndrome coronavirus 2 with high potency. *J Biol Chem* **295**, 6785-6797 (2020).

25. Wu, J., Wu, B. & Lai, T. Compassionate Use of Remdesivir in Covid-19. *N Engl J Med* **382** (2020).

26. Bago, R. *et al.* Characterization of VPS34-IN1, a selective inhibitor of Vps34, reveals that the phosphatidylinositol 3-phosphate-binding SGK3 protein kinase is a downstream target of class III phosphoinositide 3-kinase. *Biochem J* **463**, 413-427 (2014).

27. Wakil, S.J. & Abu-Elheiga, L.A. Fatty acid metabolism: target for metabolic syndrome. *J Lipid Res* **50 Suppl**, S138-143 (2009).

28. Schütter, M., Giavalisco, P., Brodesser, S. & Graef, M. Local Fatty Acid Channeling into Phospholipid Synthesis Drives Phagophore Expansion during Autophagy. *Cell* **180**, 135-149.e114 (2020).

29. Bakhache, W. *et al.* Fatty acid synthase and stearoyl-CoA desaturase-1 are conserved druggable cofactors of Old World Alphavirus genome replication. *Antiviral Res* **172**, 104642 (2019).

30. Nasheri, N. *et al.* Modulation of fatty acid synthase enzyme activity and expression during hepatitis C virus replication. *Chem Biol* **20**, 570-582 (2013).

31. Herker, E. *et al.* Efficient hepatitis C virus particle formation requires diacylglycerol acyltransferase-1. *Nat Med* **16**, 1295-1298 (2010).

32. Cao, J. *et al.* Targeting Acyl-CoA:diacylglycerol acyltransferase 1 (DGAT1) with small molecule inhibitors for the treatment of metabolic diseases. *J Biol Chem* **286**, 41838-41851 (2011).

33. Futatsugi, K. *et al.* Discovery and Optimization of Imidazopyridine-Based Inhibitors of Diacylglycerol Acyltransferase 2 (DGAT2). *J Med Chem* **58**, 7173-7185 (2015).

34. Sims, A.C. *et al.* Severe acute respiratory syndrome coronavirus infection of human ciliated airway epithelia: role of ciliated cells in viral spread in the conducting airways of the lungs. *J Virol* **79**, 15511-15524 (2005).

35. Sims, A.C., Burkett, S.E., Yount, B. & Pickles, R.J. SARS-CoV replication and pathogenesis in an in vitro model of the human conducting airway epithelium. *Virus Res* **133**, 33-44 (2008).

36. Nagy, P.D., Strating, J.R. & van Kuppeveld, F.J. Building Viral Replication Organelles: Close Encounters of the Membrane Types. *PLoS Pathog* **12**, e1005912 (2016).

37. Sasvari, Z. & Nagy, P.D. Making of viral replication organelles by remodeling interior membranes. *Viruses* **2**, 2436-2442 (2010).

504 38. den Boon, J.A. & Ahlquist, P. Organelle-like membrane compartmentalization of
505   positive-strand RNA virus replication factories. *Annu Rev Microbiol* **64**, 241-256 (2010).
506 39. Santiago, F.W. *et al.* Hijacking of RIG-I signaling proteins into virus-induced
507   cytoplasmic structures correlates with the inhibition of type I interferon responses. *J Virol*
508   **88**, 4572-4585 (2014).
509 40. Morris, D.H., Yip, C.K., Shi, Y., Chait, B.T. & Wang, Q.J. Beclin 1-Vps34 Complex
510   Architecture: Understanding the Nuts and Bolts of Therapeutic Targets. *Front Biol*
511   *(Beijing)* **10**, 398-426 (2015).
512 41. Chude, C.I. & Amaravadi, R.K. Targeting Autophagy in Cancer: Update on Clinical
513   Trials and Novel Inhibitors. *Int J Mol Sci* **18** (2017).
514 42. Dowdle, W.E. *et al.* Selective VPS34 inhibitor blocks autophagy and uncovers a role for
515   NCOA4 in ferritin degradation and iron homeostasis in vivo. *Nat Cell Biol* **16**, 1069-1079
516   (2014).
517 43. Backer, J.M. The intricate regulation and complex functions of the Class III
518   phosphoinositide 3-kinase Vps34. *Biochem J* **473**, 2251-2271 (2016).
519 44. Guo, L. *et al.* Autophagy Negatively Regulates Transmissible Gastroenteritis Virus
520   Replication. *Sci Rep* **6**, 23864 (2016).
521 45. Gassen, N.C. *et al.* SKP2 attenuates autophagy through Beclin1-ubiquitination and its
522   inhibition reduces MERS-Coronavirus infection. *Nat Commun* **10**, 5770 (2019).
523 46. Wakil, S.J. Fatty acid synthase, a proficient multifunctional enzyme. *Biochemistry* **28**,
524   4523-4530 (1989).
525 47. Schcolnik-Cabrera, A. *et al.* Orlistat as a FASN inhibitor and multitargeted agent for
526   cancer therapy. *Expert Opin Investig Drugs* **27**, 475-489 (2018).
527 48. Heaton, N.S. *et al.* Dengue virus nonstructural protein 3 redistributes fatty acid synthase
528   to sites of viral replication and increases cellular fatty acid synthesis. *Proc Natl Acad Sci*
529   *U S A* **107**, 17345-17350 (2010).
530 49. Wilsky, S. *et al.* Inhibition of fatty acid synthase by amentoflavone reduces
531   coxsackievirus B3 replication. *Arch Virol* **157**, 259-269 (2012).
532 50. Tang, W.C., Lin, R.J., Liao, C.L. & Lin, Y.L. Rab18 facilitates dengue virus infection by
533   targeting fatty acid synthase to sites of viral replication. *J Virol* **88**, 6793-6804 (2014).
534 51. Gordon, D.E. *et al.* A SARS-CoV-2 protein interaction map reveals targets for drug
535   repurposing. *Nature* **583**, 459-468 (2020).
536 52. Olzmann, J.A. & Carvalho, P. Dynamics and functions of lipid droplets. *Nat Rev Mol*
537   *Cell Biol* **20**, 137-155 (2019).
538 53. Matsuda, D. *et al.* Anti-atherosclerotic activity of triacsin C, an acyl-CoA synthetase
539   inhibitor. *J Antibiot (Tokyo)* **61**, 318-321 (2008).
540 54. Rossi Sebastiano, M. & Konstantinidou, G. Targeting Long Chain Acyl-CoA Synthetases
541   for Cancer Therapy. *Int J Mol Sci* **20** (2019).
542
543

544   **FIGURE LEGENDS**

545   **Figure 1. Standardization of an electrical resistance-based assay as a measure of SARS-**

546   **CoV-2 induced CPE and anti-SARS-CoV-2 activity.** VeroE6 cells were seeded into a

547   CytoView-Z 96-well plate and cells were allowed to stabilize overnight, as measured by

548   electrical resistance. **A)** SARS-CoV-2 was titrated in 10-fold dilutions ranging from 10-0.0001

549   MOI. Resistance was measured every minute over the course of 72 hours. Solid lines indicate the

550   mean, dotted lines indicate the standard error of three replicates.   B) Median time to death

551   calculations based on raw resistance data for each MOI. **C)** Remdesivir was titrated in 6-fold

552   dilutions ranging from 50-0.006 µM. After infection at an MOI of 0.01, resistance was

553   monitored for 48 h.p.i. and **D)** percent inhibition was determined at the 48 hour timepoint.

554

555   **Figure 2. VPS34 inhibitors exhibit anti-SARS-CoV-2 activity.** VeroE6 cells were seeded into

556   a CytoView-Z 96-well plate, and cells were allowed to stabilize overnight. Cells were pre-treated

557   with serial half-log dilutions of **A)** VPS34-IN1 or **C)** PIK-III and infected with SARS-CoV-2 at

558   an MOI=0.01. Resistance **(A and C)** was measured every minute over the course of 48 hours and

559   percent inhibition **(B and D)** was determined at the 48-hour timepoint. Solid lines indicate mean,

560   dotted lines indicate the standard error of two replicates.

561

562   **Figure 3. Screening of fatty acid inhibitors for potential anti-SARS-CoV-2 activity.** VeroE6

563   cells were seeded into a CytoView-Z 96-well plate and allowed to stabilize overnight. Cells were

564   pre-treated with serial half-log dilutions of **A)** Orlistat or **B)** Triacsin C and infected with SARS-

565   CoV-2 at an MOI=0.01. Resistance **(A and C)** was measured every minute over the course of 48

566   hours and percent inhibition **(B and D)** was determined at the 48-hour timepoint. Solid lines

567   indicate the mean and dotted lines indicate the standard error of two replicates.

568

569   **Figure 4. Single treatment of VPS34 inhibitors have potent anti-viral activity against**

570   **SARS-CoV-2.** VeroE6 cells were seeded into a CytoView-Z 96-well plate, and allowed to

571   stabilize overnight. **A)** Timeline for the time-of-addition experiment. **B)** VeroE6 cells were pre-

572   treated for one hour and compound was removed (-1), pre-treated for one hour with compound

573   maintained throughout infection (+1), or treated at 2 (+2) or 4 (+4) hours post-infection with an

574   MOI of 0.01. Resistance was measured every minute over the course of 48 hours and percent

575   inhibition was determined at the 48-hour timepoint. Data is representative of the mean and

576   standard error of three technical replicates.

577

578   **Figure 5. Attenuation of VPS34 kinase activity and fatty acid metabolism inhibit SARS-**

579   **CoV-2 replication in human airway epithelial cell line.** Calu-3 cells were plated onto a 96-

580   well plate and allowed to reach 95% confluency. Cells were then pre-treated with a range of

581   concentrations of **A-B)** VPS34-IN1, **C-D)** PIK-III, **E-F)** Orlistat, **G-H)**, Triacsin C, DMSO, or

582   mock-treated with media alone for 1 hour then infected with SARS-CoV-2 at an MOI of 0.01.

583   Supernatants were collected at 48 h.p.i. and virus was quantified by plaque assay on VeroE6

584   cells. The data is reported as plaque forming units per milliliter (pfu/ml) **(left panels).** Cell

585   viability over 48 hours was determined in parallel. Percent inhibition, IC50, and IC90 were

586   calculated from the plaque assay data and plotted with the cell viability data **(right panels).** The

587 dotted line labeled DMSO indicates the level of virus growth in the DMSO control. The dotted

588 line labeled LOD indicates the limit of detection of the plaque assay.

589

590 **Figure 6. VPS34 activity and fatty acid metabolism are required to form SARS-CoV-2 N**

591 **replication centers.** Calu-3 cells were pre-treated with VPS34-IN1 (5uM), PIK-III (5uM),

592 Orlistat (500uM), or Triacsin C (50uM) for 1 hour and infected with SARS-CoV-2 at MOI of

593 0.01. Cells were fixed at 24 h.p.i. and immunofluorescence was performed using primary

594 antibodies against SARS-CoV-2 N or dsRNA, and AlexaFluor488 or AlexaFluor647 conjugated

595 secondary antibodies, respectively. Nuclei were stained with Hoeschst 33342. Representative

596 images are shown.

597

598 **Supplemental Figure 1. Inhibition of DGATs does not prevent SARS-CoV-2 replication.**

599 VeroE6 cells were seeded into a CytoView-Z 96-well plate and allowed to stabilize overnight.

600 Cells were pre-treated with serial half-log dilutions of **A)** TC863 or **B)** PF06424439 and infected

601 with SARS-CoV-2 at an MOI=0.01. Resistance was measured every minute over the course of

602 48 hours and percent inhibition relative to the DMSO control was determined at the 48-hour

603 timepoint.

604

605 **Supplemental Figure 2. Inhibition of alpha PI3K does not prevent SARS-CoV-2**

606 **replication.** Calu-3 cells were plated onto a 96-microplate and allowed to reach 95% confluency.

607 Cells were then pre-treated with a range of concentrations of BYL719 and infected with SARS-

608 CoV-2 at an MOI of 0.01. Supernatants were collected at 48 h.p.i. and titered on VeroE6 cells

609   (left panel). Cell toxicity was determined in parallel and percent inhibition extrapolated from

610   plaque assay data (right panel).

611

612   **Supplemental Figure 3. SARS-CoV-2 N and nascent viral RNA co-localize with the**

613   **autophagy membrane marker LC3.** VeroE6 cells were infected with SARS-CoV-2. At 24

614   h.p.i., cells were pre-treated with actinomycin D followed by a 5-ethynyl uridine (EU) chase for

615   4 hours. **A)** Cells were fixed, EU labeled viral nascent RNA was detected with click chemistry,

616   and immunofluorescence performed using primary antibodies against SARS-CoV-2 N or LC3

617   and AlexaFluor488- or AlexaFluor647- conjugated secondary antibodies, respectively. Nuclei

618   were stained with Hoeschst 33342. Representative images are shown. **B)** Co-localization was

619   analyzed with Zen Blue.
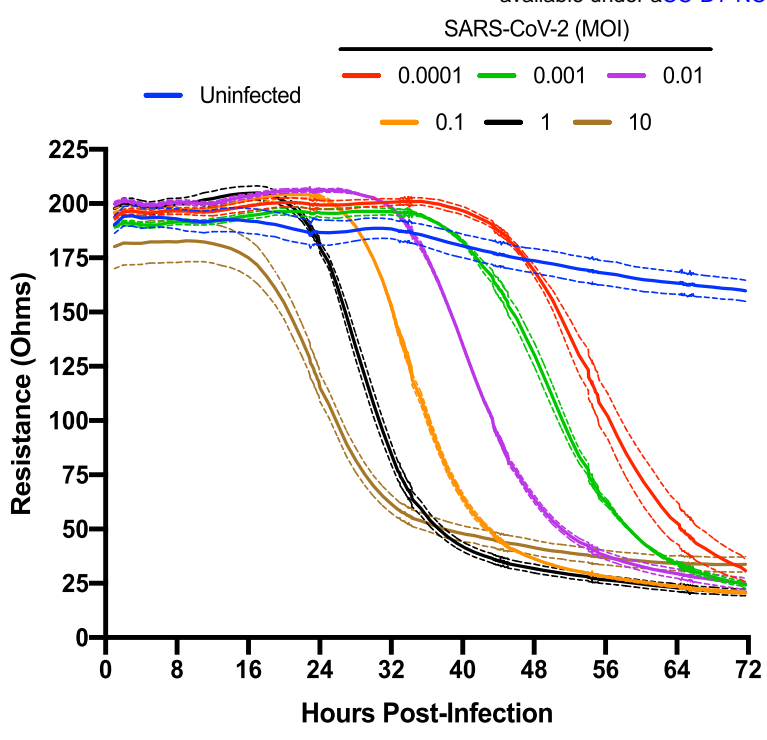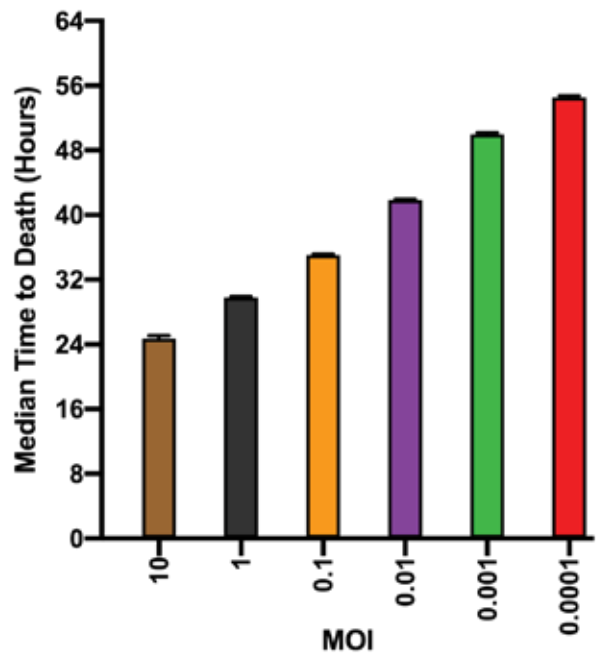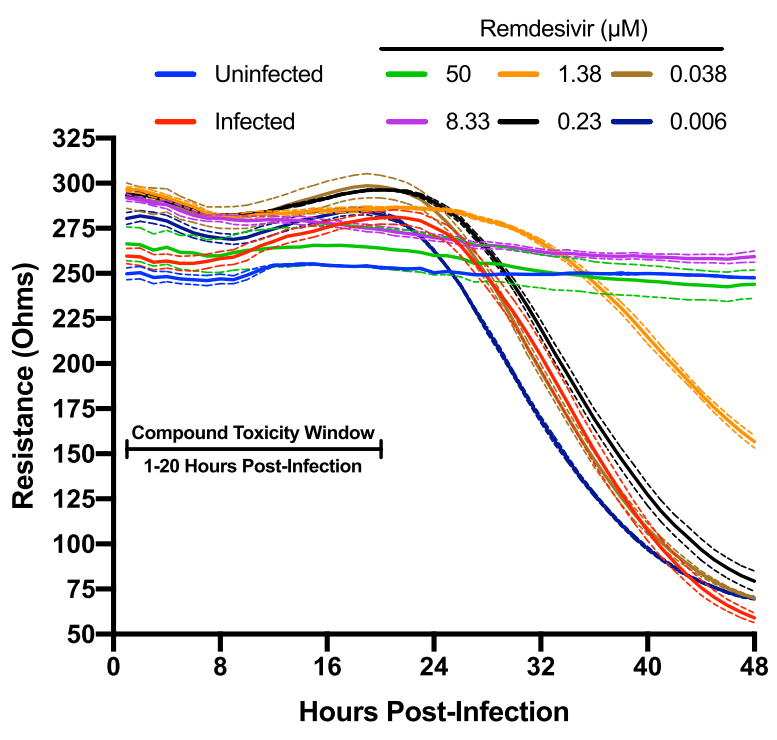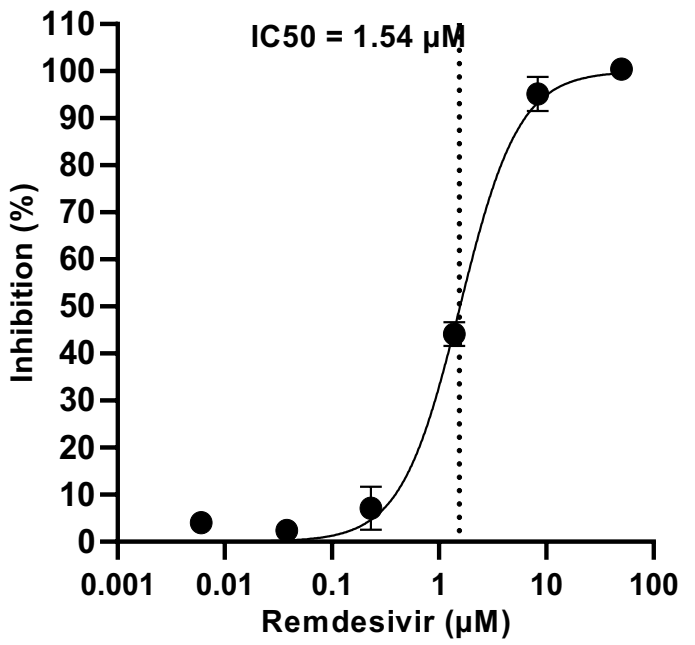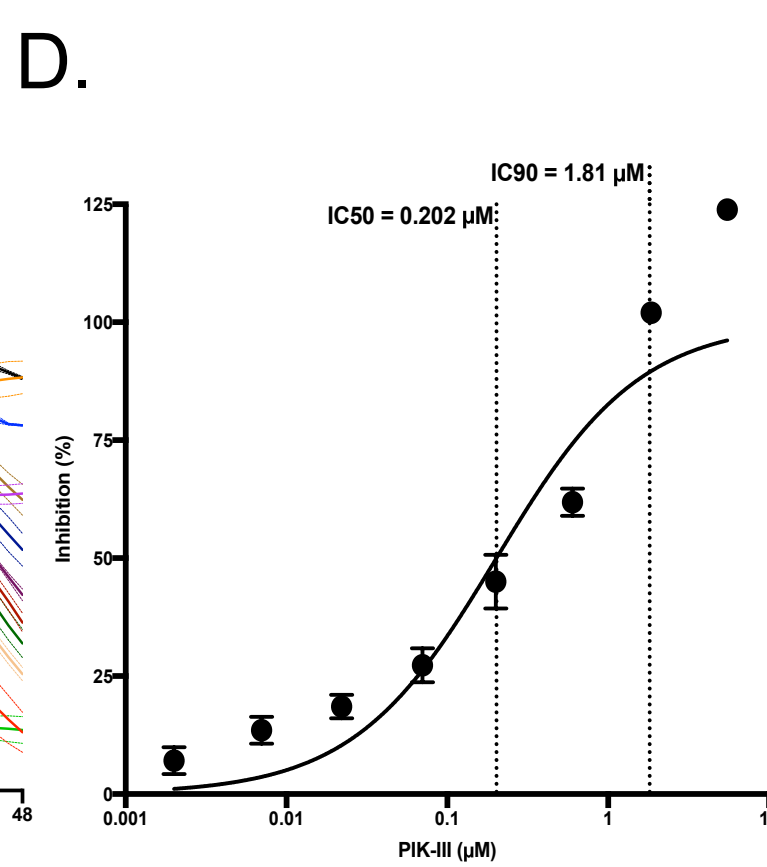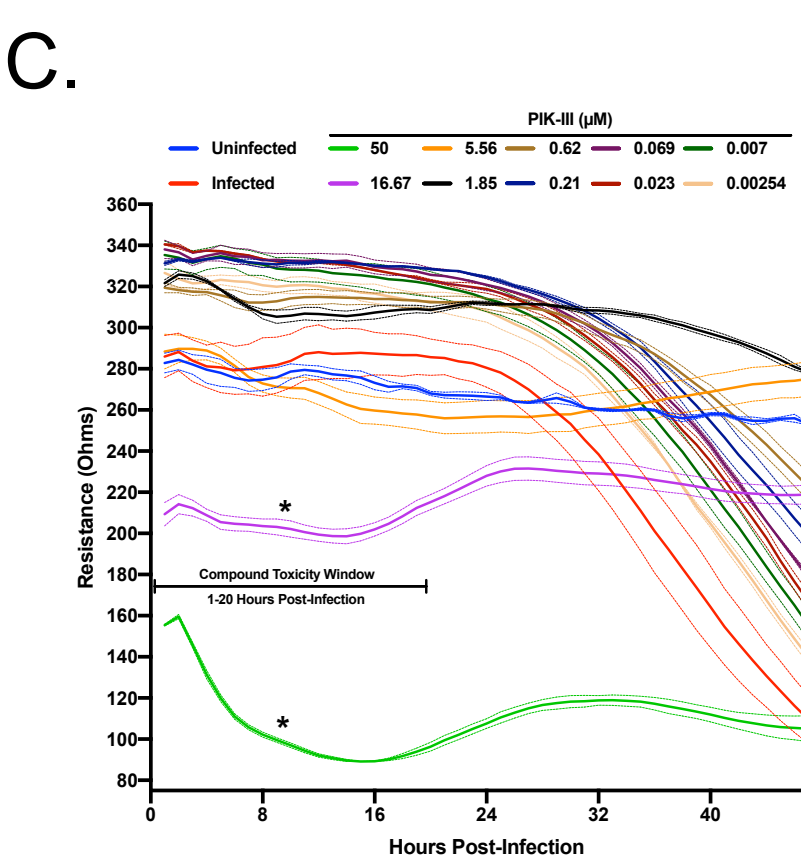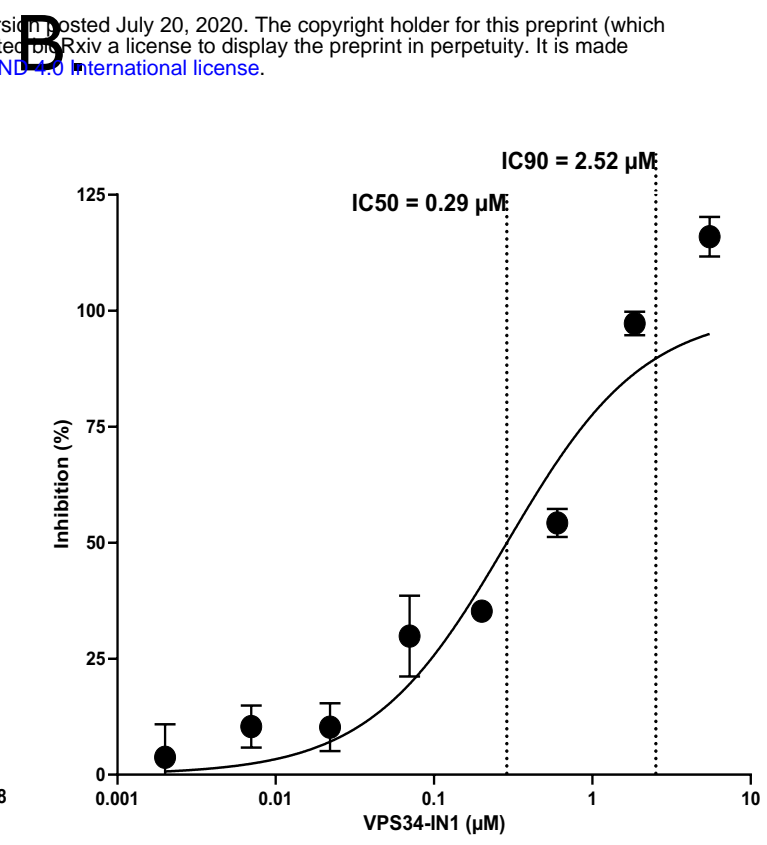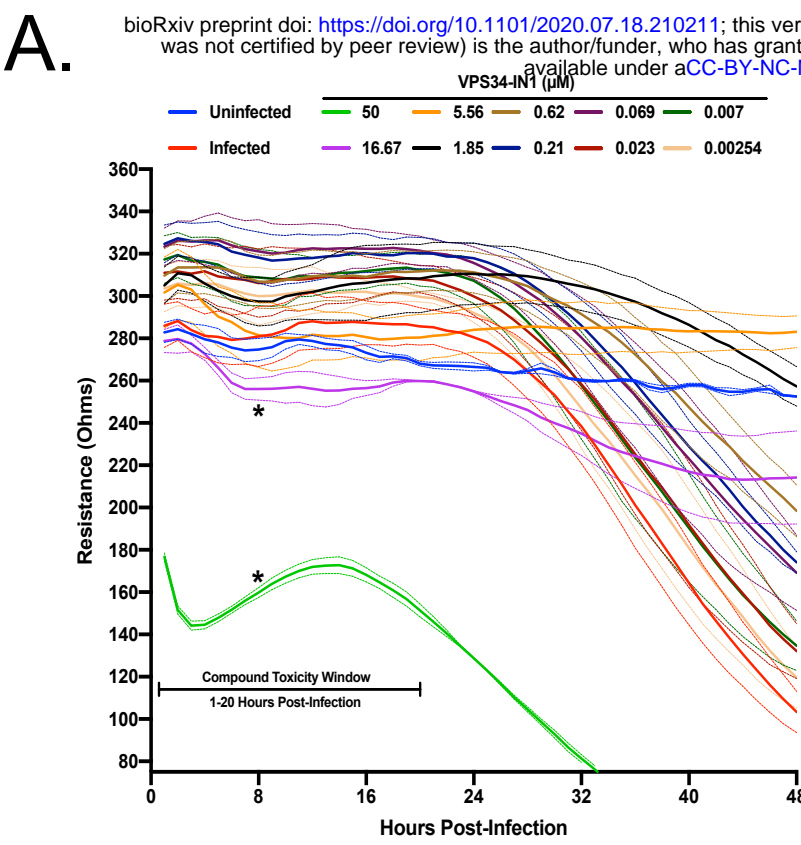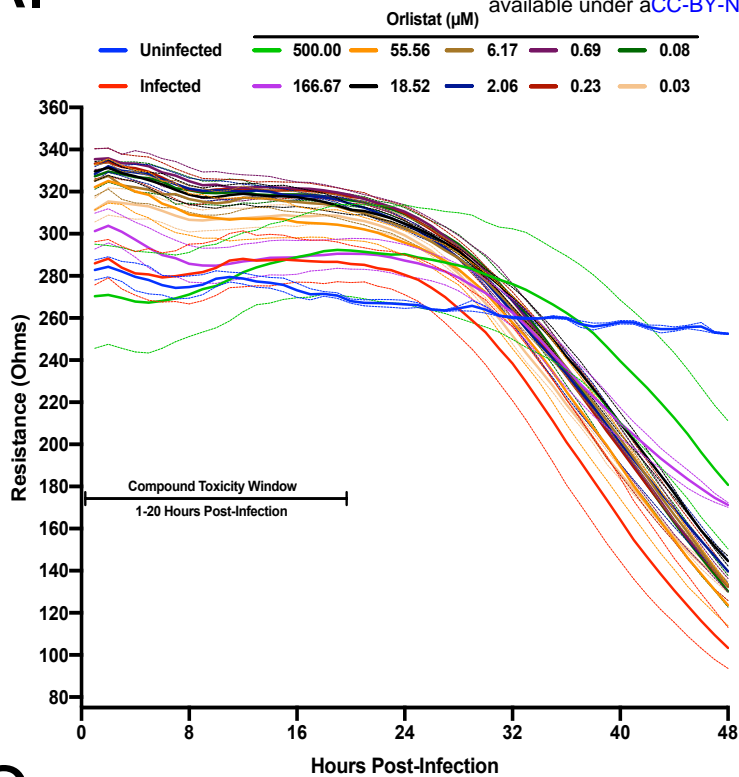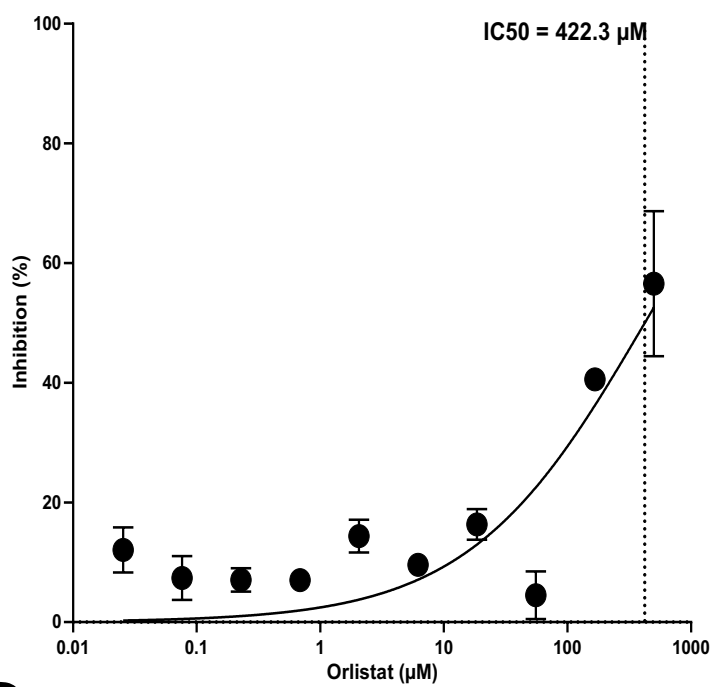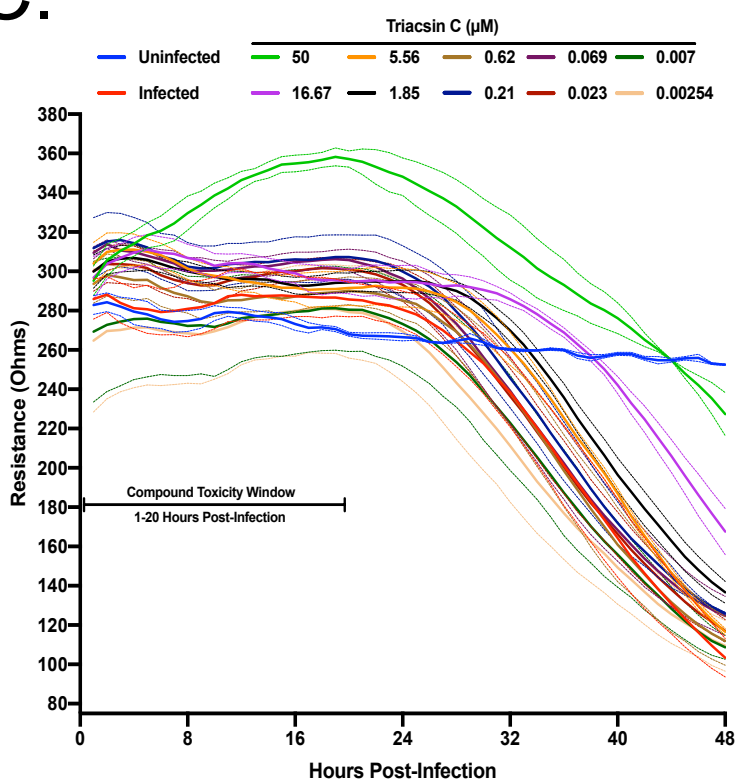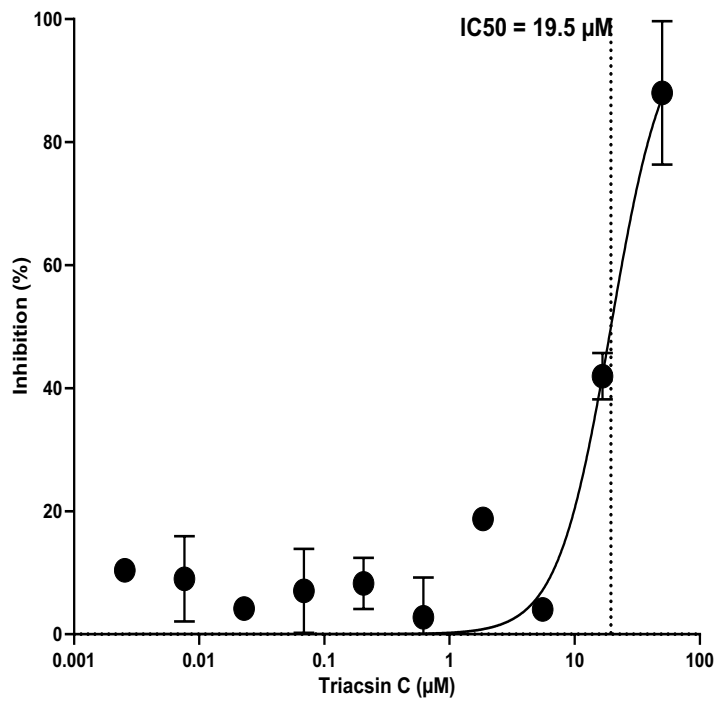
Figure 1.
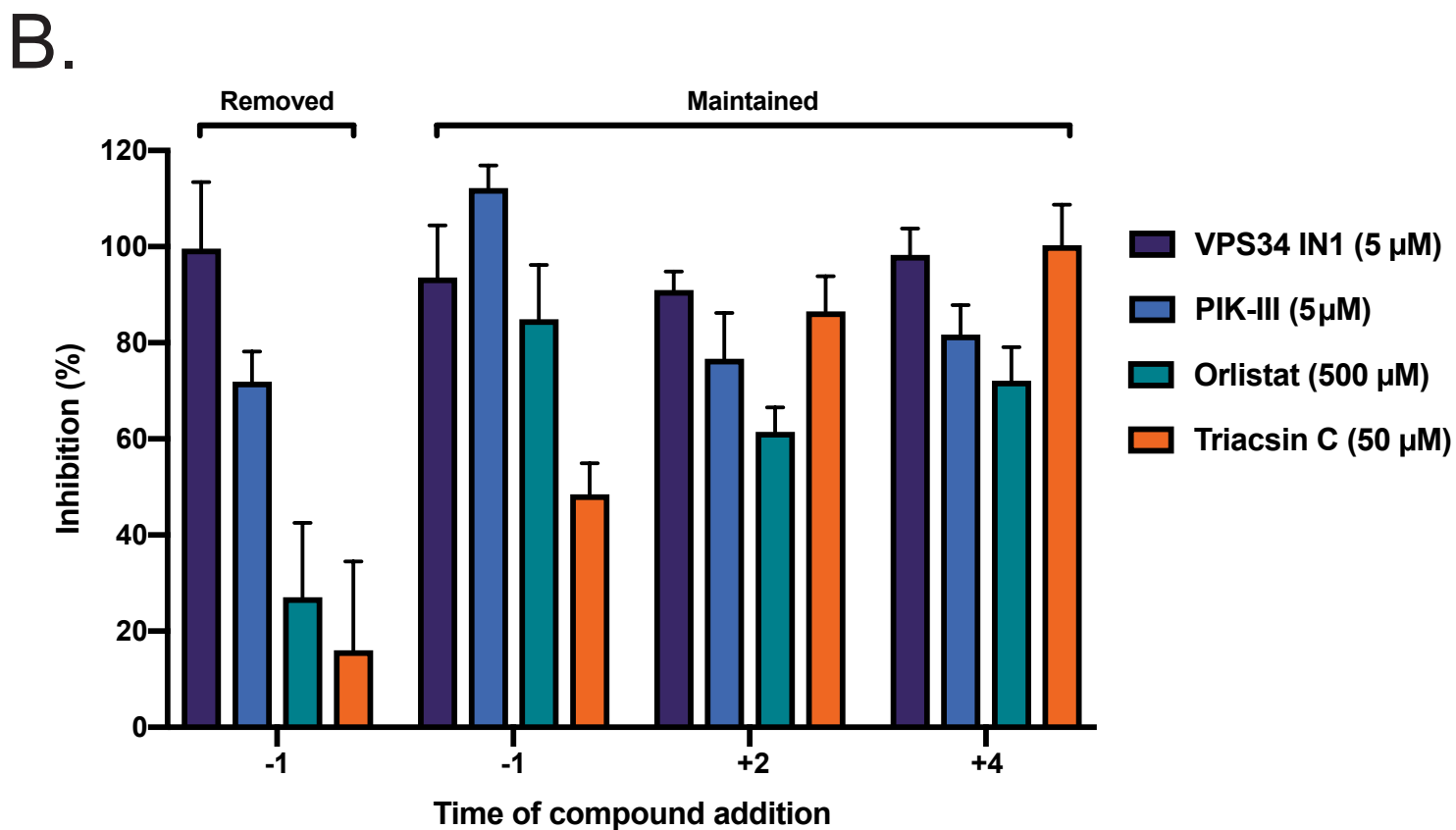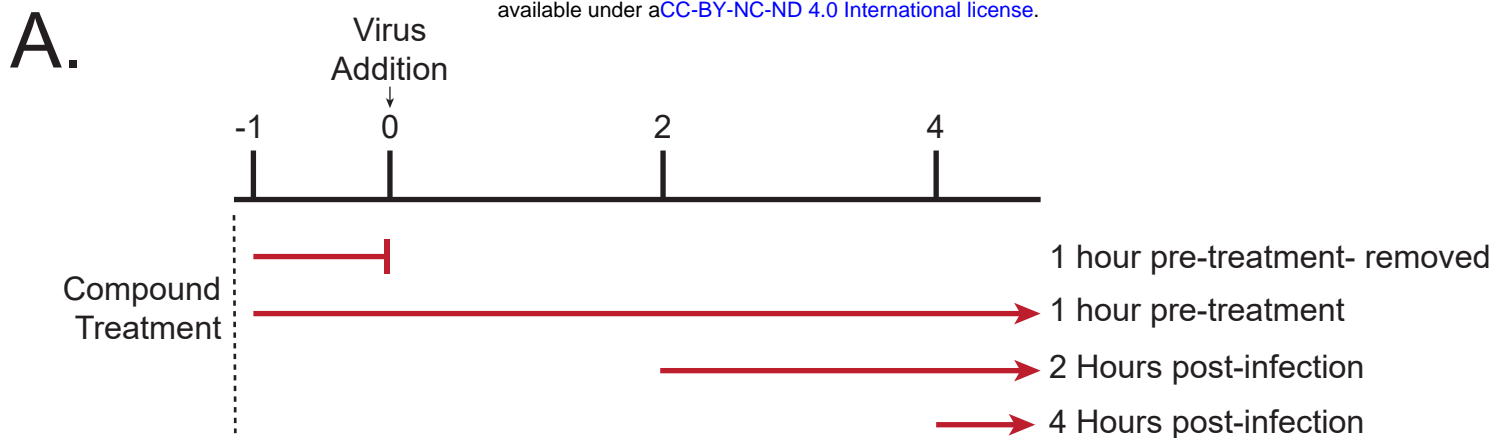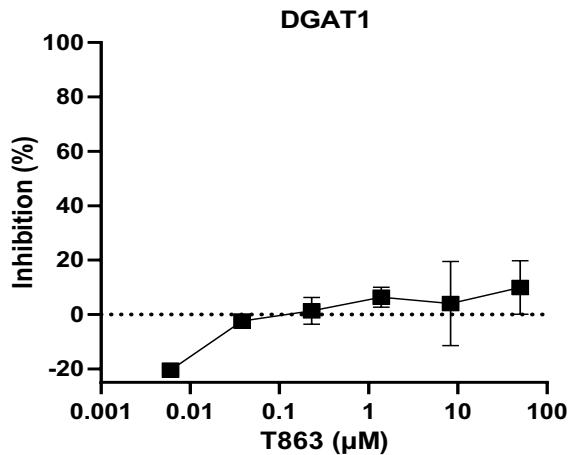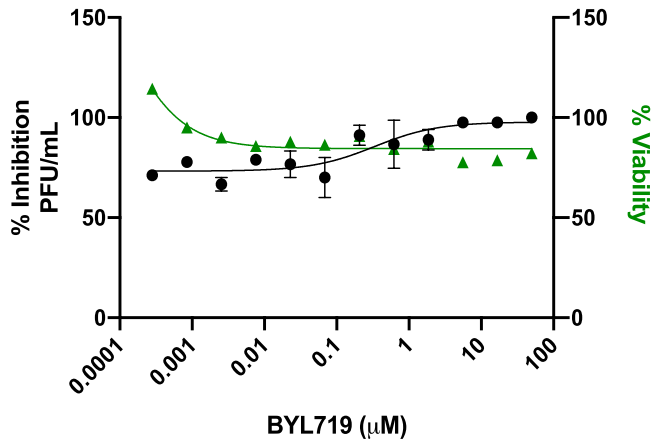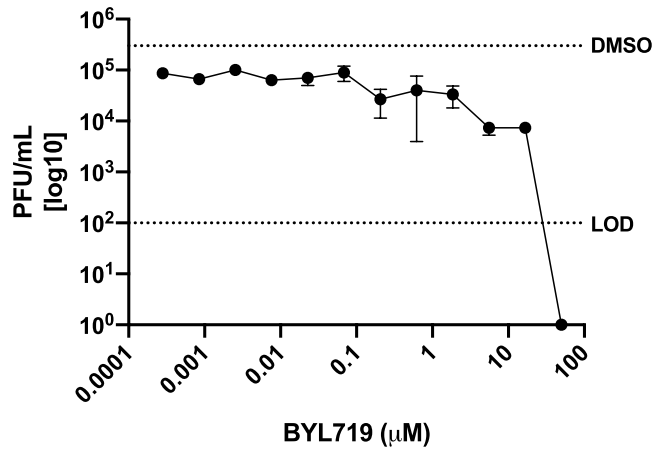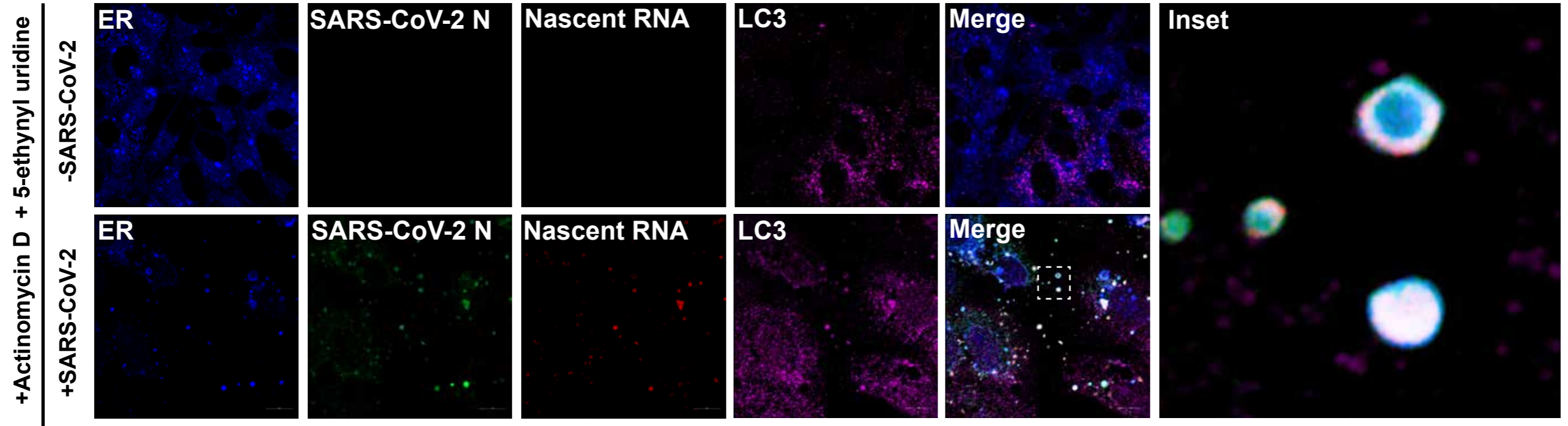
Figure 2.
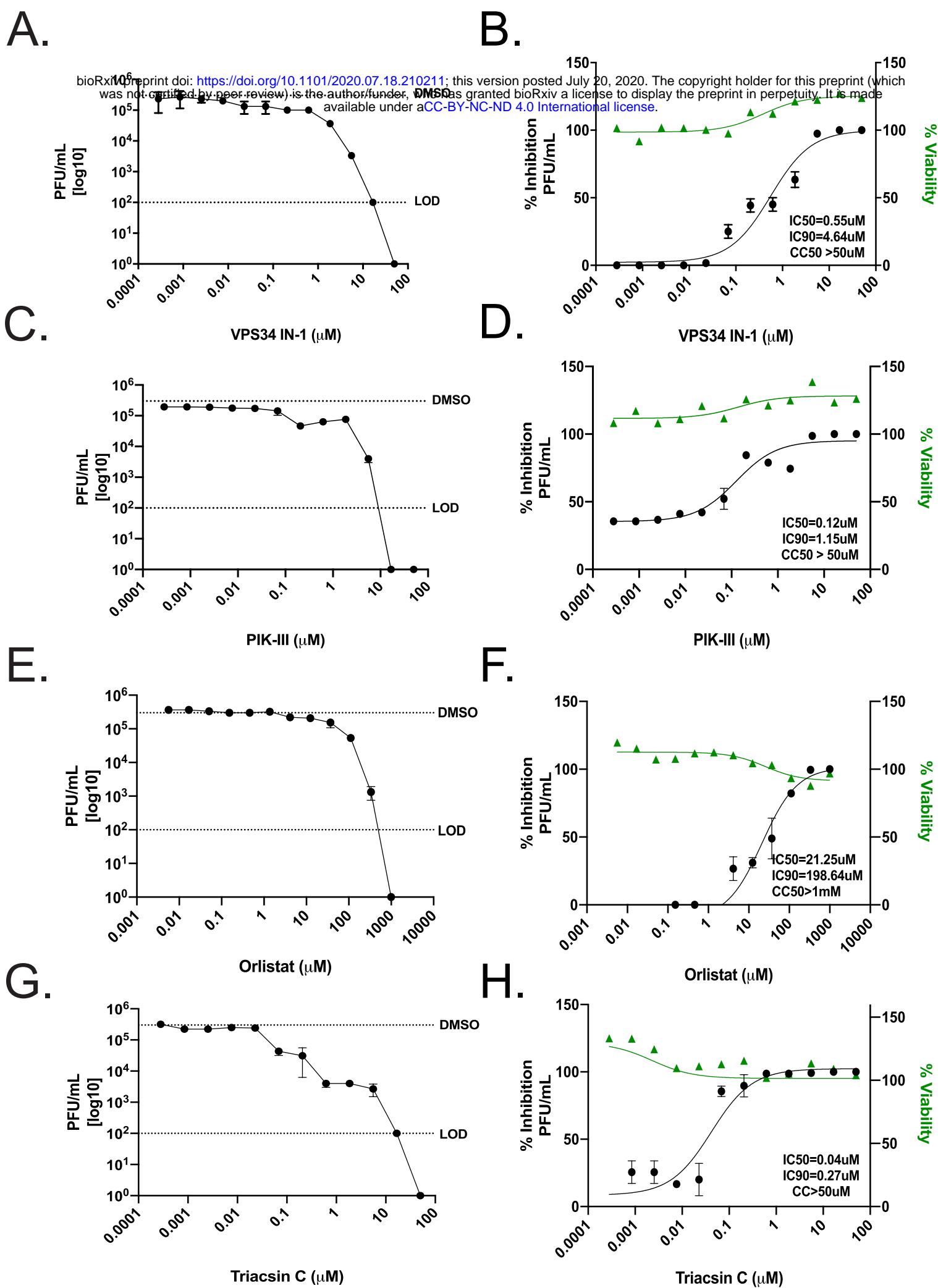
Figure 3.

Figure 4.

Figure 5.
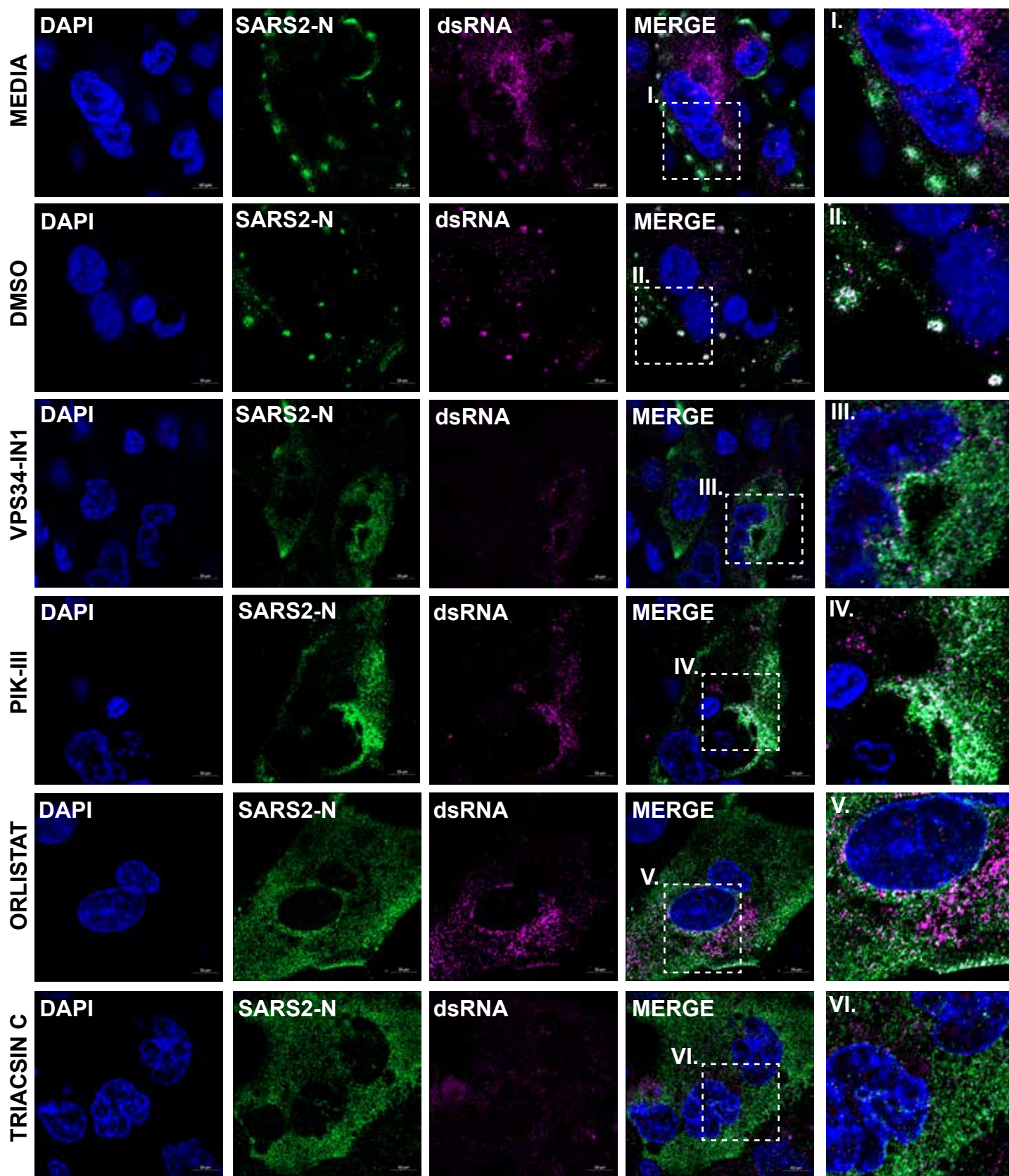
Figure 6.
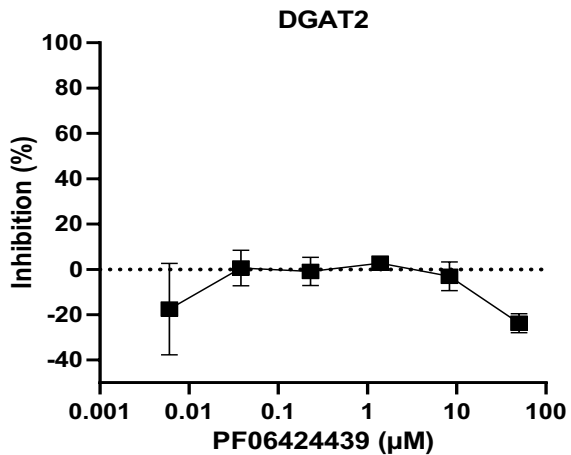
Supplemental Figure 1.

Supplemental Figure 2.

A.

ER | SARS-CoV-2 N | Nascent RNA | LC3 | Merge | Inset

-SARS-CoV-2

ER | SARS-CoV-2 N | Nascent RNA | LC3 | Merge

+SARS-CoV-2

+Actinomycin D + 5-ethynyl uridine

B.

RNA vs SARS-CoV-2 N

RNA vs LC3

Supplemental Figure 3.